AIMS Materials Science, 11(3): 585–601.
DOI: 10.3934/matersci.2024029
Received: 23 May 2024
Revised: 06 June 2024
Accepted: 13 June 2024
Published: 19 June 2024

https://www.aimspress.com/journal/Materials

Research article

Characterization of the hybrid joint between AA2024-T3 alloy and thermoplastic composite obtained by oxy-fuel welding (OFW)

Rafael Resende Lucas[1,*], Rita de Cássia Mendonça Sales-Contini[2], Luis Felipe Barbosa Marques[1], Jonas Frank Reis[1], Ana Beatriz Ramos Moreira Abrahão[3], Edson Cocchieri Botelho[1] and Rogério Pinto Mota[1]

[1] São Paulo State University (UNESP), School of Engineering and Sciences, Guaratinguetá, São Paulo 12516-410, Brazil
[2] Aeronautical Structures Laboratory, Technological College of São José dos Campos Prof. Jessen Vidal (FATEC), São José dos Campos, São Paulo 12247-014, Brazil
[3] Electrochemistry and Corrosion Laboratory, Technological College of Pindamonhangaba (FATEC), Pindamonhangaba, São Paulo 12445-010, Brazil

* **Correspondence:** Email: rr.lucas@unesp.br; Tel: +55-12-98120-9031.

Abstract: Studies on dissimilar materials joining have greatly increased, transitioning from temporary to permanent joining methods. The latter approach is more applicable due to the hybrid structure offering the best properties of the constituent materials, along with the development of new materials and manufacturing procedures. In this study, the AA2024-T3 alloy was treated with plasma electrolytic oxidation (PEO) and a thermoplastic composite/AA2024-T3 hybrid joint was manufactured using oxy-fuel welding (OFW). Morphological aspects, chemical compositions electrochemical and mechanical properties of hybrid composite joints were determined. The results indicated that the joint exhibits a uniform structure. The adhesion between the dissimilar materials reached a strength of 4.2 to 5.2 MPa, with cohesive bonding and without severe degradation of the thermoplastic matrix in some cases. It was observed that PEO treatment decreased the interface shear strength due to the high silicon content presence in the coating. The coatings effectively increased nobility and corrosion resistance, with corrosion rates ranging from 0.0087 to 0.018 mm/year.

Keywords: welding; aluminum; composite; PEO; characterization

1. Introduction

Thermoplastic composite materials are continuously evolving, improving the manufacturing process, applications, and union, such as welding with other materials. Welding dissimilar materials can be challenging due to the mechanical and thermal differences of the materials applied in the structure. Points that should be considered for the effective union include the selection of the welding process, surface preparation, temperature control, pressure control, and whether or not there is additional material [1–6].

Aluminum alloys are widely used in several fields, such as aerospace structures (for instance, the alloy AA2024-T3) in plates, fuselages, bulk scales, lower wings, etc. The mechanical resistance of the alloy value is equal to or greater than medium carbon structural steel alloys due to precipitation hardening of Cu-Al_2 and $CuMgAl_2$ phases [7–9].

Protective coatings deposition techniques must be developed to mitigate localized corrosion and increase abrasion resistance and anchoring points in the AA2024-T3 alloy. Plasma electrolytic oxidation (PEO) has attracted the attention of several researchers and technology companies. The process of PEO is like conventional anodizing but with higher potentials (>100 V), allowing the use of environmentally friendly electrolytes and a much shorter processing time (of the order of seconds). PEO produces oxide coatings with higher physical and chemical properties than the conventional process [9–13].

Although thermoset composites are more employed in aeronautical market structures, thermoplastic composites, such as glass fiber-reinforced polyetherimide, have a promising future. They have high impact resistance, stabilized thermal properties, and high energy absorption capacity, which makes them attractive for applications in aerospace structures. Easy processing is also an important factor because it allows the production of parts with high dimensional precision, which is fundamental in aerospace structures [1,14,15].

Dissimilar materials can be united in several ways, which fall basically into two categories: permanent union and movable union. In a permanent union, the separation of materials is not possible without damaging them. The most common technique for a mobile union is the use of screws to join subsets, which is rarely used for high-value structures, such as aeronautical ones [16,17].

Among the permanent union processes, melting welding has achieved promising results due to the efficiency in the samples´ preparation, such as welding. This simple process entails the preparation of the chamfer, the heating of the material above the glass transition temperature of the polymer matrix (217 °C) in the case of the polyetherimide matrix, and the application of pressure to ensure the union [16,18,19].

Few studies have been published on the melting process for welding dissimilar materials and/or thermoplastic composites due to some complications inherent in the process, such as controlling the flame temperature within the working limits for the polymer matrix. In the mid-2010s, authors such as Abrahão et al. [16] developed feasibility studies of the union of composite materials and hybrid structures by welding OFW (oxy welding). Lucas and colleagues [15] conducted a study aimed at optimizing the PEO process using a 2^3 experimental design. The study achieved an improvement twice as high compared to the welding of untreated materials.

In this study, the AA2024-T3 alloy was joined with a glass fiber-reinforced polyetherimide thermoplastic composite using the OFW process with LPG (liquefied petroleum gas). To improve adhesion, the PEO process was applied. The joints and their shear strength values were then characterized.

The relevance of this study was to verify the feasibility of the oxy-fuel welding process (a cheaper process) for dissimilar materials, such as aluminum and thermoplastic composite, and to explore environmentally friendly processes to improve the alloy's surface properties.

Although there are studies in the literature applying anodization to aluminum alloys, they mainly address conventional treatment processes, using acids and/or more expensive methods such as laser. Additionally, many studies employ specific adhesives that, although effective, tend to increase the mass of the final structure. These methods, despite being widely used, have disadvantages in terms of cost, complexity, and environmental impact. Thus, the search for more economical and environmentally friendly alternatives becomes essential, especially for joining dissimilar materials such as aluminum and thermoplastic composites, which will be addressed in this study.

2. Materials and methods

2.1. Preparation of samples

AA2024-T3 alloy strips were cut in the dimensions 100 × 25 × 3.5 mm (based on ASTM D1002:19) [20]. Then, they were ultrasonically cleaned with distilled water and neutral detergent for 900 s, followed by cleaning with isopropyl alcohol for 900 s. The alloy chemical composition, according to the supplier, is shown in Table 1.

Table 1. Chemical composition AA2024-T3 by mass (%).

Cr	Cu	Fe	Mg	Mn	Si	Ti	Zn	Al
<0.1	3.8–4.9	<0.5	1.2–1.8	0.3–0.9	<0.5	<0.15	<0.25	balance

Samples of the thermoplastic composite reinforced with glass fiber were cut into the same dimension with a bandsaw, and a sander was used to remove the sharp edges.

2.2. PEO treatment

The surface treatment processes for aluminum aim to improve surface properties, including corrosion resistance and, for this study, to increase adhesion. The system used was an electrolytic stainless-steel tank (AISI 430) and an AC voltage variation with a rectifier/bender circuit. The treatment was performed by varying the immersion time between 120, 210, and 300 s with a constant voltage of 380 VDC (potentiostatic method). The electrical system is present in Figure 1. To ensure a treated surface area of 625 mm^2, an experimental resource of electrical tape was placed in areas that would not be treated.

A sodium silicate-based solution (Na_2SiO_3—15 g/L) was prepared with a sodium phosphate additive (Na_3PO_4—1.5 g/L), and the solution was subjected to ultrasound homogenization for 900 s. Using pH indicator paper, a pH of 13 was verified.

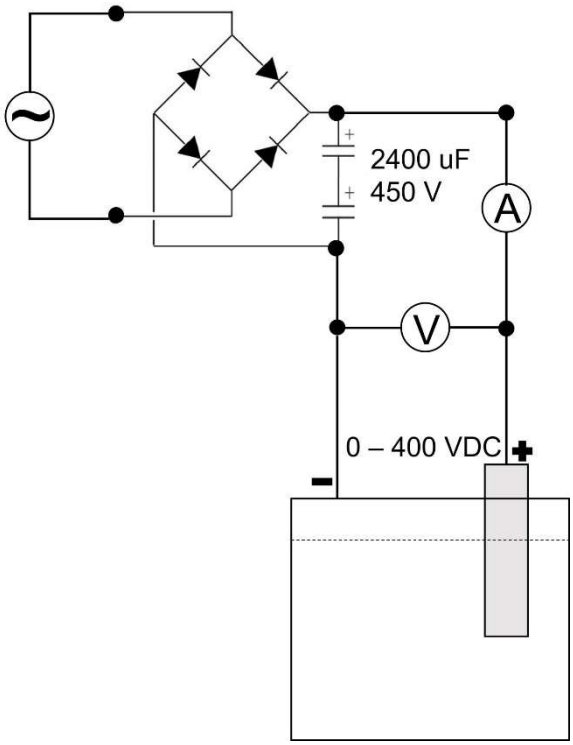

Figure 1. Experimental system for PEO treatment.

2.3. Samples' welding

The equipment employed to bond materials by welding is common in mechanical workshops, which include a bottle of LPG and manometers to control the output pressure of the gas. We used 5 psi, as shown in Figure 2.

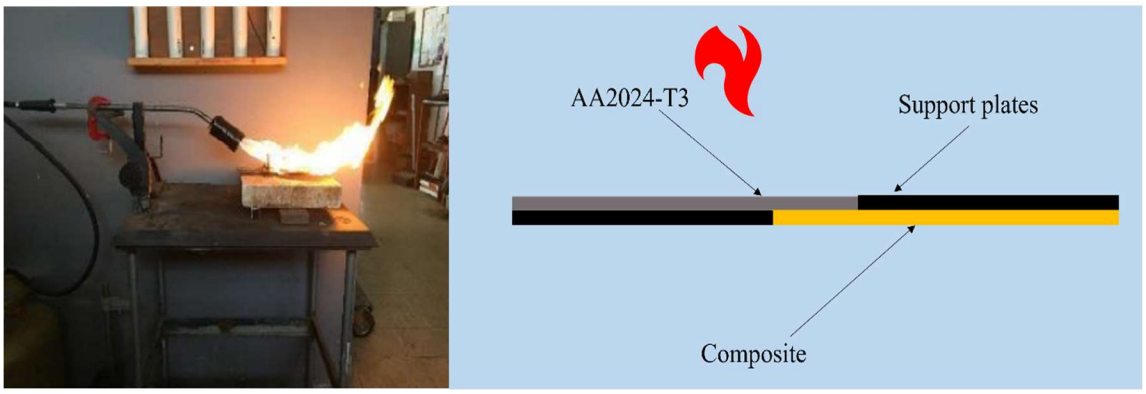

Figure 2. Welding of aluminum samples with thermoplastic composite.

For welding to occur in the best possible way. The samples were mounted in a "sandwich" system attached with adapted staples constructed by the authors to ensure good surface contact between the

samples. The flame contact time on the treated aluminum sample was about 105 s, and the distance between the torch nozzle and the aluminum sample was 50 mm.

When the flames were turned off, the surface temperature of the aluminum sample must be evaluated to determine whether the polyetherimide glass transition temperature was reached and that there was "glued" with the oxide coating. For this, an infrared thermocouple, MINIPA MT 395, with a measuring range of 50–1650 ℃ and accuracy of 0.1 °C, was used.

2.4. Characterizations of coatings and hybrid joint

The morphological and chemical compositions of the oxide coatings generated were performed by scanning electron microscopy (SEM), and by energy dispersive spectroscopy (EDS), VEGA3 TESCAN model, with electron acceleration of 25kV and working distance (WD) of 15.76 mm. The characterization occurred with backscattered electron detectors (BSE), which allows the analyses of the chemical elements' atomic numbers present in the function of the sample contrast. To evaluate the composite/anodized aluminium interface, i.e. the region of failure between the polymer matrix and the aluminium, a 2 mp digital electron microscope, KNUP, model 8012, with 500× magnification was used.

To evaluate the shear strength of the hybrid joint, the mechanical characterization followed the ASTM D1002:2010 standard [20]. In a SHIMADZU AG-X equipment, with a load module of 50 kN and displacement of 1.5 mm/min (0.059 in./min), four measurements were performed for each set.

To evaluate the alloy corrosion resistance as received and after PEO treatment, the samples were subjected to the electrochemical techniques of linear polarization and impedance using the potentiostat/galvanostat AUTOLAB model PGSTAT302N from Metrohm Autolab©. The tests were conducted in a horizontal electrochemical cell with a 3.5% NaCl solution and assembled with three electrodes: alloy-treated AA2024-T3 (working electrode), platinum (counter electrode), and Ag/AgCl (saturated KCl—reference electrode). One replicate was performed for each sample, with each sample being immersed in the solution for approximately 900 s (at open circuit potential). The linear polarization test was conducted at a scan rate of 0.33 mV/s, with an analysis range of +700 to −300 mV relative to the open circuit potential (OCP) value.

3. Results and discussion

3.1. Morphology and composition of PEO coatings

Figure 3 shows SEM' microscopy of oxide coatings. The coatings generated by the PEO did not present uniform morphology, which is a typical characteristic of the electrical regime type applied to the treatment. The scratches from the sanding process of the samples were evident. Some coating regions exhibit microstructures characteristic of the PEO process, such as bubbles with microcracks due to rapid cooling with the solution (red arrows) [21–26].

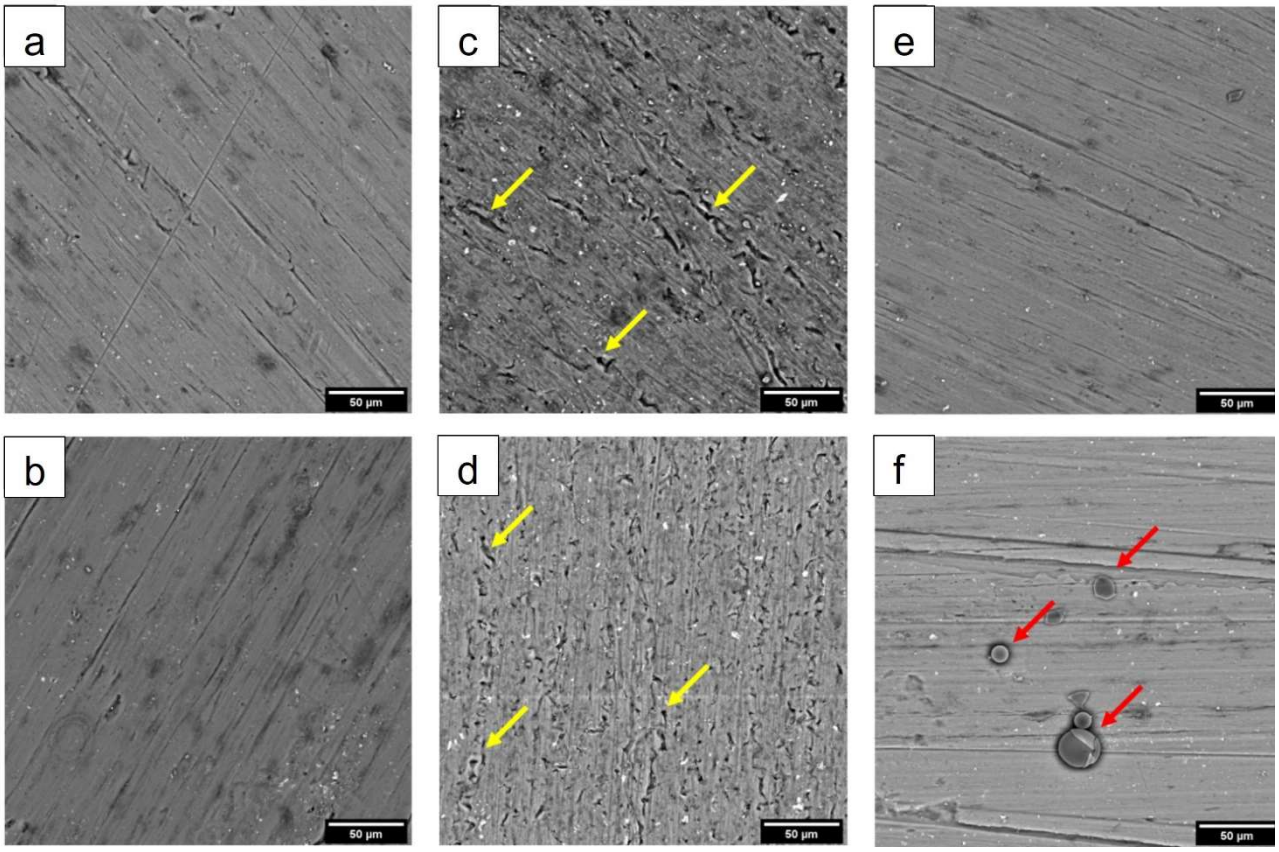

Figure 3. SEM of PEO coatings (a/b: 120 s; c/d: 210 s, and e/f: 300 s).

The sample treated for 210 s (C/D) showed better characteristics of PEO coatings, such as a more porous surface (yellow arrows), due to the presence of micro arcs in the treatment. However, the sample treated for 300 s (E/F) presented morphological characteristics similar to that treated for 120 s, probably due to the presence of isolated regions of electric arcs during treatment that ruptured the coating generated up to 210 s, with no time to form a new coating by 300 s [15,24,27].

To complement the SEM analysis, the number of elements in the coatings was determined using dispersive energy spectroscopy. Table 2 presents an average evaluation of the elements and indicates that the coating is mainly composed of aluminum and oxygen (Al_2O_3). The electrolyte elements added to the coating, although in a smaller amount, were also observed [15,24].

Table 2. Chemical composition of PEO coatings.

%	120 s/380 V	210 s/380 V	300 s/380 V
Al	64.6	65.1	43.6
O	28.9	32.5	41.5
C	3.6	1.2	-
Si	1.5	0.9	8.1
Fe	0.2	0.1	0.2
Na	0.9	-	3.4
P	0.1	0.1	0.2
Cr	0.1	-	-
Cu	0.1	0.1	0.1
Zn	0.1	0.1	0.1

The electrolyte elements presence in the oxide coating is evident in the ionic dissolution of electrolytes, such as Na_2SiO_3 (Eq 1) and Na_3PO_4 (Eq 2).

$$Na_2SiO_3 \rightarrow 2Na^{+}_{(aq)} + SiO_3^{-2} \quad (1)$$

$$Na_3PO_{4(aq)} \rightarrow 3Na^{+}_{(aq)} + PO^{-3}_{4(aq)} \quad (2)$$

During dissociation, negative ions (SiO_3^{-2} and PO_4^{-3}) are attracted to the positive pole (AA2024) in the solution and then incorporated into the forming coating. Although the Na ion is positive, a sodium-containing electrolyte is also incorporated because of the micro-discharge channels in the forming coating.

In a previous study [24], these coatings were characterized by x-ray diffraction (XRD), to analyze the crystalline composition of the coatings, noting that they presented peaks related to aluminum, amorphous alumina, gamma alumina (Al_2O_3) and mullite ($3Al_2O_3 \cdot SiO_2$). The mullite is needle-shaped and appears when the Si content on the surface is higher as was the case with the sample treated for 300 s. Using the eddy current for thickness evaluation, the coatings presented 0.2, 1.3, and 1.2 μm of thickness for coatings treated by 120, 210, and 300 s, respectively.

3.2. Shear strength test

After welding the anodized aluminum samples with the thermoplastic composite material, the set was submitted to lap shear test, according to ASTM D1002:10 standard [20] (Table 3).

Table 3. Shear test values (MPa).

	AA2024-T3	120 s/380 V	210 s/380 V	300 s/380 V
MPa	5.2 ± 2.2	4.2 ± 0.7	5.2 ± 3.1	4.8 ± 1.8

It is observed that the shear strength of the composite/anodized aluminum interfaces before joining did not show an improvement, but rather a decrease or maintenance of the strength, as was the case with the 210 s/380 V treatment. This decrease in strength can be explained by the high silicon content in the coating, which makes the surface brittle when subjected to shear stress. This same phenomenon has already been observed in the literature [14,21].

Figure 4 shows a correlation between the silicon content in the coatings and the average shear strength values of the interfaces.

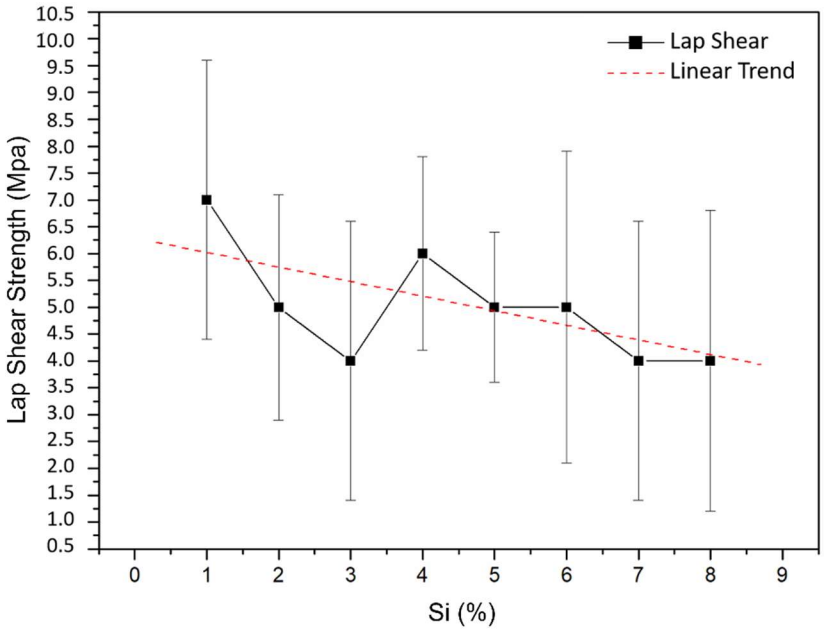

Figure 4. Silicon content vs. shear stress.

As the silicon strength increased, the adhesive strength reduced between the coating and the polymeric matrix. This increase also led to a decrease in the Al_2O_3 phases, which are extremely important for the O–H groups' formations. These groups, in turn, enhanced the coating moisture absorption capacity, facilitating hydrogen bonding with the polymeric matrices [10,14,15,24].

The micrography (Figure 5) suggests that the samples with better shear resistance (C and D, 210 s/380 V) had a higher concentration of the polymer matrix anchored in aluminum after joint failure. On the other hand, samples A and B (120 s/380 V) and E and F (300 s/380 V) had a lower concentration of the polymeric matrix anchored, resulting in a lower shear resistance. Considering ASTM D55733-99 (2019) standard [28], to classify the joints' failure modes, we found that there was a mixed failure, involving three types: adhesive failure (ADH), cohesive failure (COH), and thin-layer cohesive failure (TLC). The adhesive failure, indicated in Figure 5 by the red arrows, represented approximately 84.6%, 36.3%, and 59.7% for the sets treated for 120, 210, and 300 s, respectively. The cohesive failure, indicated by the yellow arrows, showed a polymer matrix rupture, representing an effective bond of 15.4%, 63.8%, and 40.3% for the samples treated for 120, 210, and 300 s, respectively. The thin layer cohesive failure (black arrows) was identified in the samples treated for 120 and 300 s, representing residues from the composite's polymer matrix composite.

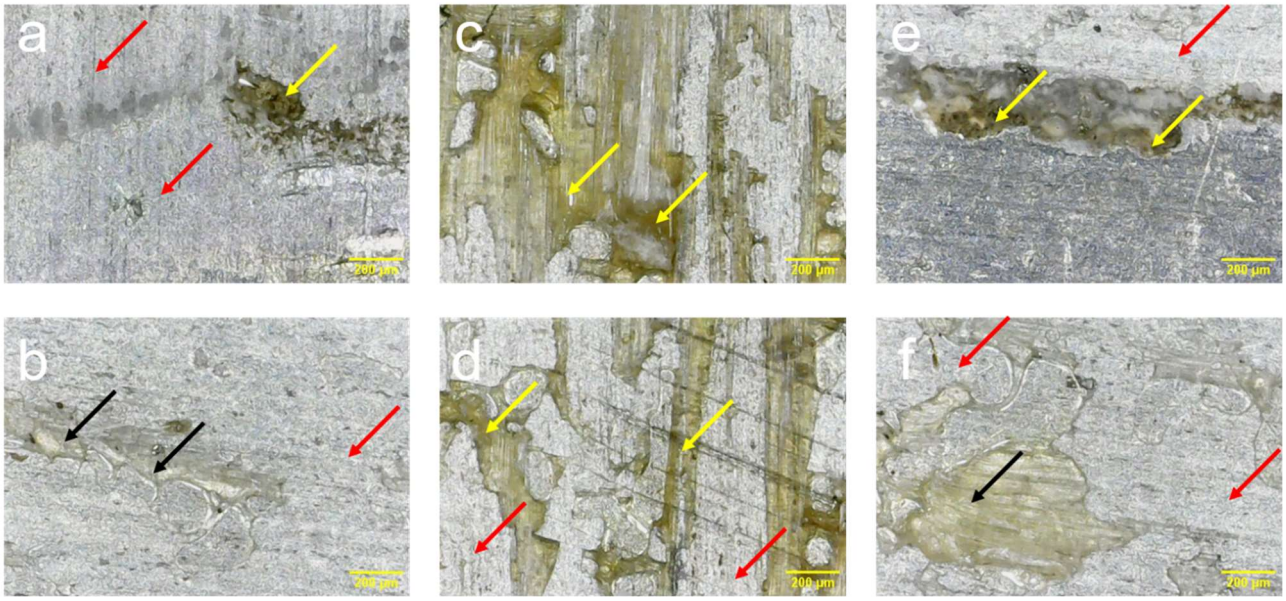

Figure 5. Microscopic images from the hybrid joints after lap shear tests: a/b: 120 s; c/d: 210 s, and e/f: 300 s (magnification of 500×).

Figure 6 shows images from the composite/anodized aluminum interface. The sample treated for 120 s (A and B) showed poor mechanical anchoring, delamination of the composite material, detachment at the interface, and microcracks in the oxide coating, as reported in the literature [29–32].

The sample treated for 210 s (C and D) showed better mechanical anchoring, with no cracks, delamination, or voids at the interface. On the other hand, the sample treated for 300 s (E and F) showed a darker coloration (yellow circle) in the thermoplastic matrix, which may indicate the beginning of the thermal degradation process. The oxygen presence during the welding process may have caused premature local degradation of the composite, even if the polymeric matrix degradation temperature, indicated by the supplier, was not reached [33–35].

In addition, in a previous study [24], the coating synthesized for 210 s showed an average roughness of 0.5 µm, being higher than in the samples treated for 120 and 300 s, which had a roughness of 0.45 and 0.40 µm, respectively. Inferring adhesion by mechanical anchoring.

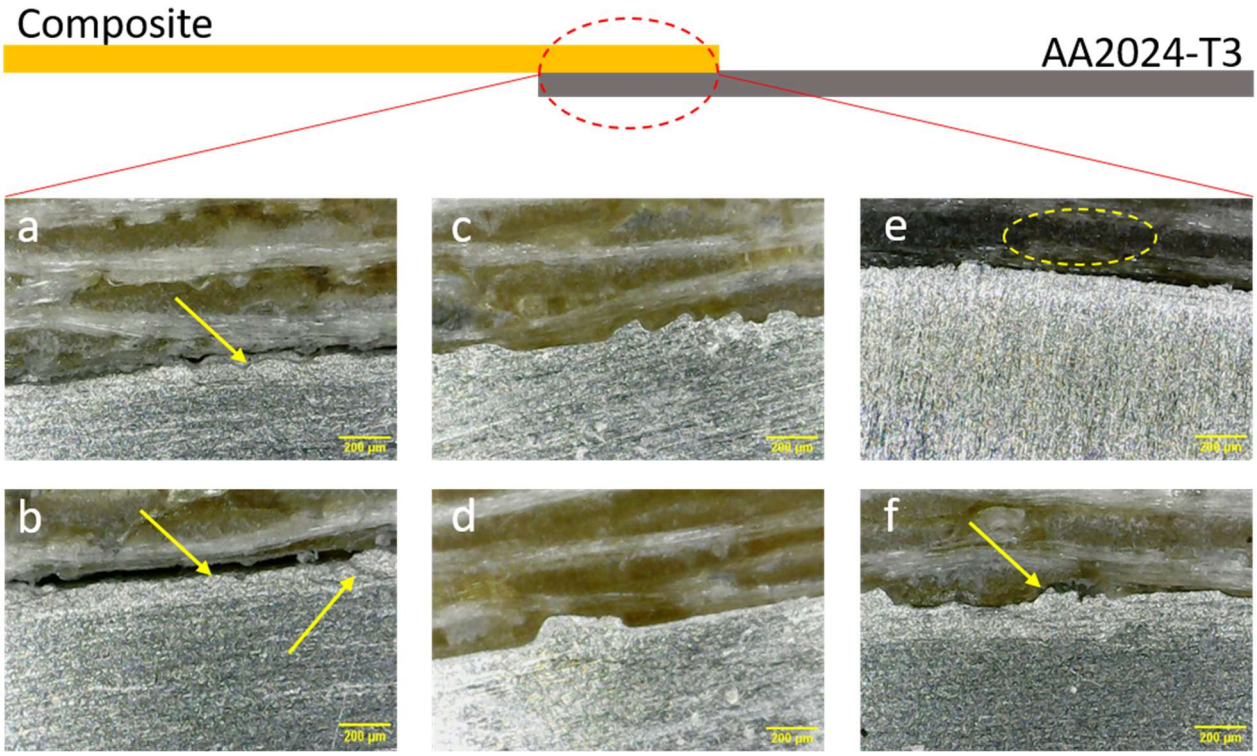

Figure 6. Micrographic image from hybrid joint weld region: a/b: 120 s; c/d: 210 s, and e/f: 300 s (magnification of 500×).

3.3. Corrosion resistance

Figure 7 presents polarization curves of the untreated sample and the samples subjected to the treatments. The corrosion parameters are summarized in Table 4, where E_{corr} and I_{corr} represent the corrosion potential and the corrosion current density of the sample, respectively.

In general, samples with lower E_{corr} values are more susceptible to corrosion, as curves that shift to the right indicate a higher corrosion rate. Figure 6 and Table 4 suggest that the samples treated for 120 and 210 s by the PEO process had increased nobility compared to the untreated alloy. However, the treatment performed for 300 s was not as noble, possibly due to the presence of microcracks, allowing ions to reach the aluminum substrate, leading to corrosion [10,22,36,37].

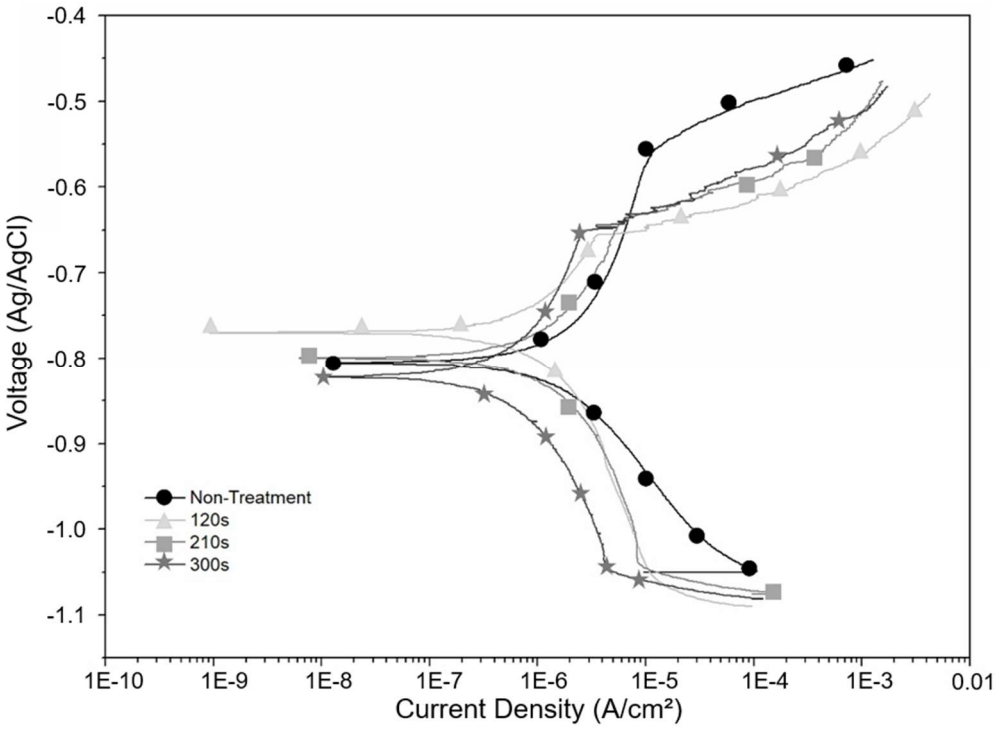

Figure 7. Polarization curves of AA2024-T3 alloy in its as-received state and after PEO treatment.

Table 4. Corrosion parameter values.

	AA2024-T3	120 s	210 s	300 s
Ecorr (V)	–0.80	–0.77	–0.79	–0.82
Icorr($\mu A \cdot cm^{-1}$)	2.990	1.587	1.245	0.769
mm/y	0.0334	0.0180	0.0141	0.0087

The sample treated for 210 s achieved the best performance for corrosion applications. Figure 8 shows the Nyquist plot, in which larger semicircles are observed for samples treated for 210 and 300 s. This information helps to elucidate the samples' corrosion mechanisms, as the larger the semicircle, the greater the resistance to corrosion [21,22].

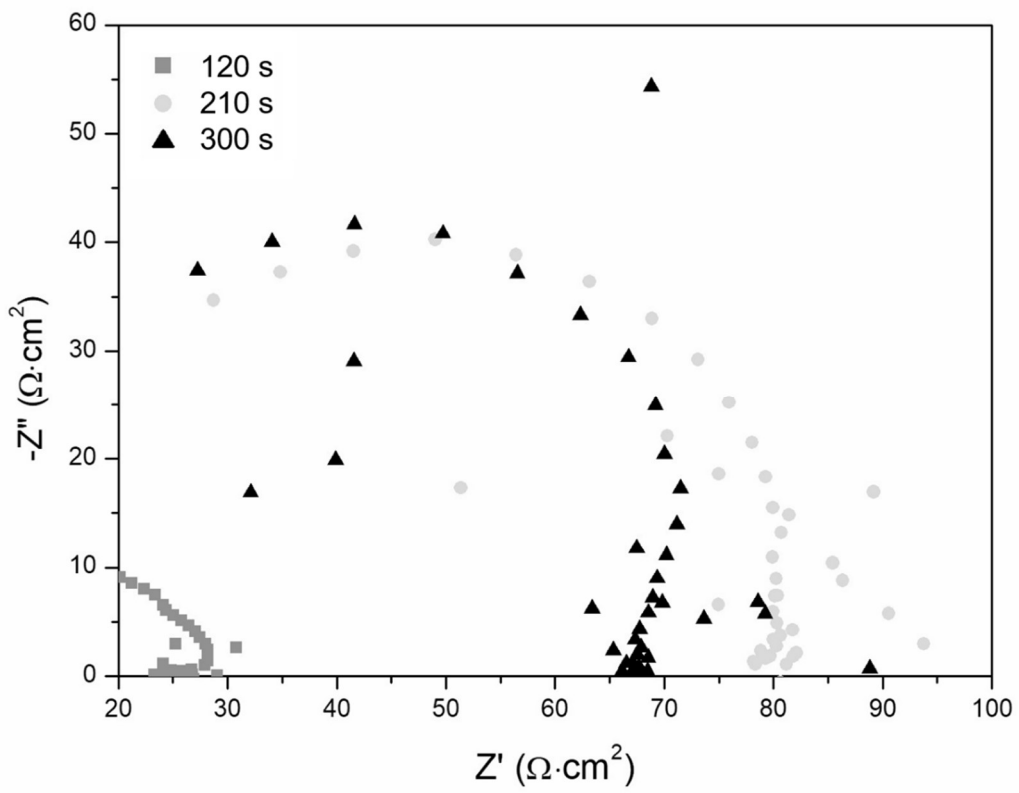

Figure 8. Nyquist graphic of samples treated by PEO.

Considering the oxidation mechanism of aluminum in a NaCl solution, initially, aluminum oxidizes, forming Al^{3+} ions (Eq 3). Moreover, the reduction of dissolved oxygen in the solution occurs (Eq 4), completing the overall reaction of aluminum oxidation (Eq 5).

$$Al_{(s)} \rightarrow Al^{3+}_{(aq)} + 3e^{-} \quad (3)$$

$$O_{2(g)} + 2H_2O_{(l)} + 4e^{-} \rightarrow 4OH^{-}_{(aq)} \quad (4)$$

$$4Al_{(s)} + 3O_{2(g)} + 6H_2O_{(l)} \rightarrow 4Al^{3+}_{(Aq)} + 12OH^{-}_{(Aq)} \quad (5)$$

In the presence of Cl^{-} ions, the aluminum hydroxide formed from Eq 5 reacts to form soluble aluminum chloride (Eq 6).

$$Al(OH)_3 + 3Cl^{-} \rightarrow AlCl_3 + 3OH^{-} \quad (6)$$

The Cl^{-} ions penetrate the pores of the aluminum oxide layer (Al_2O_3) and promote its dissolution. With the continuous process of removal and formation of this layer, uniform or localized oxidation, such as pitting, occurs [38–40].

In this study, the Bode graphs showed a lack of consistency, compromising the precision of coatings corrosion analysis by this method.

4. Conclusions

In this study, PEO was used to evaluate its feasibility in improving adhesion between dissimilar materials and increasing corrosion resistance of susceptible alloys, such as AA2024 T3 alloy, through oxide coating growth. Thus, it is concluded that: SEM/EDS microscopy analysis showed that the coatings generated have typical characteristics of PEO processes, such as a thin oxide layer (0.2 to 1.3 μm), pores randomly distributed on the surface, needle-shaped microstructures, mullite ($3Al_2O_3 \cdot SiO_2$) present in coatings with high Si content, and cavities with micro-cracks resulting from micro-discharges that occur during the process, for microseconds. These discharges cause localized heating (10000 to 25000 K) and are followed by rapid cooling due to contact with the electrolyte. The coating is mostly alumina (Al_2O_3), with traces of other elements, both from the samples and the electrolyte, such elements being: Fe, Cu, Cr, Zn, Si, Na, Si and P, thus demonstrating the effectiveness of the PEO process in incorporating electrolyte elements into the coating, being able to functionalize the surface as necessary.

In the overlap shear strength mechanical tests, the hybrid joints averaged 5.2; 4.2; 5.2 and 4.8 MPa for untreated samples and treated samples for 120, 210 and 300 s, respectively. Macrographic analysis revealed that joints with higher strength exhibited a higher concentration of the polymer matrix in aluminum. The increased silicon content in the coating, as observed in the samples treated for 120 and 300 s, resulted in a decrease in shear strength due to increased Si–O phases, rendering the coating brittle when subjected to shear stresses.

Electrochemical analyses confirmed the effectiveness of the treatment in increasing the nobility and improving the substrate corrosion resistance. The sample treated for 300 s showed the best resistance, with a corrosion rate of 0.0087 mm/year, representing a 74% improvement in the corrosion rate. However, there were inconsistencies in the analysis due to noise observed in the Bode plot, although it was possible to perform the Nyquist plot, which demonstrated an improvement in the corrosion resistance of the samples treated for 210 and 300 s.

We demonstrated the feasibility of welding dissimilar materials, such as aluminum and thermoplastic composite. In future research, other factors of the PEO process should be analyzed through statistical studies to optimize joint strength. Additionally, the importance of better controlling the anodization parameters to obtain more homogeneous coatings is highlighted.

Use of AI tools declaration

The authors declare they have not used Artificial Intelligence (AI) tools in the creation of this article.

Acknowledgements

The authors thank CAPES for funding the graduate program at the São Paulo State University (UNESP), and provide doctoral scholarship number: 88887.827403/2023-00, the Aeronautical Technology Institute (ITA) for the SEM/EDS characterizations, and the National Council for Scientific and Technological Development (CNPq) for providing a Project number 306576/2020-1.

Author contributions

Main experimental work and data analysis: R.R.L; R.C.M.S.C.; L.F.B.M.; J.F.R. and A.B.R.M.A.; methodology: R.R.L.; project administration: R.R.L.; E.C.B. and R.P.M.; writing—original draft: R.R.L. and R.C.M.S.C.; writing—review and editing: R.R.L. and R.C.M.S.C.

Conflict of interest

Rita De Cássia M. Sales-Contini is on a special issue editorial board for *AIMS Materials Science* and was not involved in the editorial review or the decision to publish this article. All authors declare that there are no competing interests.

References

1. Barbosa LCM, de Souza SDB, Botelho EC, et al. (2019) Fractographic evaluation of welded joints of PPS/glass fiber thermoplastic composites. *Eng Fail Anal* 102: 60–68. https://doi.org/10.1016/j.engfailanal.2019.04.032
2. Sarma K, Borah MJ, Saha N (2023) Friction stir spot welding: A novel approach to weld polyvinyl chloride. *AIP Conf Proc* 2825: 040002. https://doi.org/10.1063/5.0171424
3. Shashikumar S, Sreekanth M (2024) Investigation on mechanical properties of polyamide 6 and carbon fiber reinforced composite manufactured by fused deposition modeling technique. *J Thermoplast Compos Mater* 37: 1730–1747. https://doi.org/10.1177/08927057231200006
4. Ye J, Wu W, Gao Y, et al. (2023) Hygrothermal aging effects on fiber-metal-laminates with engineered interfaces. *Compos Commun* 43: 101721. https://doi.org/10.1016/j.coco.2023.101721
5. Siddique A, Iqbal Z, Nawab Y, et al. (2023) A review of joining techniques for thermoplastic composite materials. *J Thermoplast Compos Mater* 36: 3417–3454. https://doi.org/10.1177/08927057221096662
6. Liu Z, Li Y, Liu Y, et al. (2023) Ultrasonic welding of metal to fiber-reinforced thermoplastic composites: A review. *J Manuf Process* 85: 702–712. https://doi.org/10.1016/j.jmapro.2022.12.001
7. Tiamiyu A, Badmos A, Odeshi A, et al. (2017) The influence of temper condition on adiabatic shear failure of AA 2024 aluminum alloy. *Mater Sci Eng A* 708: 492–502. https://doi.org/10.1016/j.msea.2017.10.026
8. Zhang G, Wu L, Tang A, et al. (2018) Active corrosion protection by a smart coating based on a MgAl-layered double hydroxide on a cerium-modified plasma electrolytic oxidation coating on Mg alloy AZ31. *Corros Sci* 139: 370–382. https://doi.org/10.1016/j.corsci.2018.05.010
9. Fioravante I, Nunes R, Acciari H, et al. (2019) Films formed on carbon steel in sweet environments—A review. *J Brazil Chem Soc* 30: 1341–1349. https://doi.org/10.21577/0103-5053.20190055
10. Lucas R, Gonçalves L, Santos D (2020) Morphological and chemical characterization of oxide films produced by plasma anodization of 5052 aluminum alloy in solution containing sodium silicate and sodium phosphate. *Rev Bras Apl Vac Campinas* 39: 33–41. https://doi.org/10.17563/rbav.v39i1.1154

11. Zhou C, Qian N, Su H, et al. (2022) Effect of energy distribution on the machining efficiency and surface morphology of Inconel 718 nickel-based superalloy using plasma electrolytic polishing. *Surf Coat Technol* 441: 128506. https://doi.org/10.1016/j.surfcoat.2022.128506
12. Pezzato L, Gennari C, Franceschi M, et al. (2022) Influence of silicon morphology on direct current plasma electrolytic oxidation process in AlSi10Mg alloy produced with laser powder bed fusion. *Sci Rep* 12: 14329. https://doi.org/10.1038/s41598-022-18176-x
13. Valentini F, Pezzato L, Dabalà M, et al. (2023) Study of the effect of functionalization with inhibitors on the corrosion properties of PEO-coated additive manufactured AlSi10Mg alloy. *J Mater Res Technol* 27: 3595–3609. https://doi.org/10.1016/j.jmrt.2023.10.160
14. Shore D, Wilson J, Matthews A, et al. (2021) Adhesive bond strength of PEO coated AA6060-T6. *Surf Coat Technol* 428: 127898. https://doi.org/10.1016/j.surfcoat.2021.127898
15. Lucas R, Marques L, Botelho E, et al. (2024) Experimental design of the adhesion between a PEI/glass fiber composite and the AA1100 aluminum alloy with oxide coating produced via plasma electrolytic oxidation (PEO). *Ceramics* 7: 596–606. https://doi.org/10.3390/ceramics7020039
16. Abrahão A, Reis J, Brejão S, et al. (2015) Evaluation of time, current and pressure parameters in electrical resistance welding of PEI/continuous fiber composites: influence on mechanical resistance. *Mater* 20: 530–543. https://doi.org/10.1590/S1517-707620150002.0053
17. Maia G, Souza M, Brito A (2021) A discussion on the parameters of the resistance spot welding process and their influences on the quality of the welded joint using analysis and design of experiments. *SAE Technical Paper*. https://doi.org/10.4271/2020-36-0180
18. Faria R (2018) Use of the extended finite element method to predict the strength of hybrid T-joints. *Master Thesis*. https://recipp.ipp.pt/handle/10400.22/12703
19. Robles J, Dubé M, Hubert P, et al. (2022) Repair of thermoplastic composites: An overview. *Adv Manuf-Polym Compos Sci* 8: 68–96. https://doi.org/10.1080/20550340.2022.2057137
20. ASTM (2019) Standard test method for apparent shear strength of single-lap-joint adhesively bonded metal specimens by tension loading (metal-to-metal). Available from: https://www.astm.org/d1002-10r19.html.
21. Liu G, Lu X, Zhang X, et al. (2022) Improvement of corrosion resistance of PEO coatings on Al alloy by formation of ZnAl layered double hydroxide. *Surf Coat Technol* 441: 128528. https://doi.org/10.1016/j.surfcoat.2022.128528
22. Fatimah S, Kamil M, Han D, et al. (2022) Development of anti-corrosive coating on AZ31 Mg alloy subjected to plasma electrolytic oxidation at sub-zero temperature. *J Magnes Alloy* 10: 1915–1929. https://doi.org/10.1016/j.jma.2021.07.013
23. Aliasghari S, Rogov A, Skeldon S, et al. (2020) Plasma electrolytic oxidation and corrosion protection of friction stir welded AZ31B magnesium alloy-titanium joints. *Surf Coat Technol* 393: 125838. https://doi.org/10.1016/j.surfcoat.2020.125838
24. Lucas R, Mota R, Abrahão A, et al. (2022) Characterization of oxide coating grown by plasma electrolytic oxidation (PEO) at different times on aluminum alloy AA2024-T3. *MRS Commun* 12: 266–271. https://doi.org/10.1557/s43579-022-00174-9
25. Mohedano M, Mingo B, Matykina E, et al. (2021) Effects of pre-anodizing and phosphates on energy consumption and corrosion performance of PEO coatings on AA6082. *Surf Coat Technol* 409: 126892. https://doi.org/10.1016/j.surfcoat.2021.126892

26. Qiu X, Tariq N, Qi L, et al. (2019) Effects of dissimilar alumina particulates on microstructure and properties of cold-sprayed alumina/A380 composite coatings. *Acta Metall Sin* 32: 1449–1458. https://doi.org/10.1007/s40195-019-00917-z
27. Molaei M, Fattah-alhosseini A, Nouri M, et al. (2022) Systematic optimization of corrosion, bioactivity, and biocompatibility behaviors of calcium-phosphate plasma electrolytic oxidation (PEO) coatings on titanium substrates. *Ceram Int* 48: 6322–6337. https//doi.org/10.1016/j.ceramint.2021.11.175
28. ASTM (2019) Standard practice for classifying failure modes in fiber-reinforced-plastic (FRP) joints. Available from: https://www.astm.org/d5573-99r19.html.
29. Chai Y, Yan J, Wang C, et al. (2023) Effect of electrical parameters on the growth and properties of 7075 aluminum alloy film based on scanning micro-arc oxidation with mesh electrode. *J Mater Res Technol* 25: 988–998. https://doi.org/10.1016/j.jmrt.2023.06.020
30. Dias G, Sakundarini N, May C (2021) Mechanical and failure analysis of multi-materials adhesive joining. *Int J Integr Eng* 13: 160–166. https://doi.org/10.30880/ijie.2021.13.07.019
31. Sánchez-Romate X, Baena L, Jiménez-Suárez A, et al. (2019) Exploring the mechanical and sensing capabilities of multi-material bonded joints with carbon nanotube-doped adhesive films. *Compos Struct* 229: 111477. https://doi.org/10.1016/j.compstruct.2019.111477
32. Haddou Y, Salem M, Amiri A, et al. (2023) Numerical analysis and optimization of adhesively-bonded single lap joints by adherend notching using a full factorial design of experiment. *Int J Adhes Adhes* 26: 103482. https://doi.org/10.1016/j.ijadhadh.2023.103482
33. Wilson A, Grabowski A, Kustosik K, et al. (2018) Tartaric acid cross-contamination in post-cascade rinses after sulphuric acid anodising (SAA): Effect on adhesive bond strength of AA6060-T6 alloy. *Int J Adhes Adhes* 81: 30–35. https://doi.org/10.1016/j.ijadhadh.2017.11.004
34. Müller-Pabel M, Agudo J, Gude M (2022) Measuring and understanding cure-dependent viscoelastic properties of epoxy resin: A review. *Polym Test* 114: 107701. https://doi.org/10.1016/j.polymertesting.2022.107701
35. Ramgobin A, Fontaine G, Bourbigot S (2019) Thermal degradation and fire behavior of high performance polymers. *Polym Rev* 59: 55–123. https://doi.org/10.1080/15583724.2018.1546736
36. Posuvailo V, Imbirovych N, Povstyanoy O, et al. (2023) The state of electrolytic plasma in synthesis of oxide ceramic coatings on the magnesium basis, In: Ivanov V, Pavlenko I, Liaposhchenko O, et al. *Advances in Design, Simulation and Manufacturing VI. DSMIE 2023. Lecture Notes in Mechanical Engineering*, Cham: Springer, 258–269. https://doi.org/10.1007/978-3-031-32774-2_26
37. Fattah-alhosseini A, Chaharmahali R, Alizad S, et al. (2023) Corrosion behavior of composite coatings containing hydroxyapatite particles on Mg alloys by plasma electrolytic oxidation: A review. *J Magnes Alloy* 11: 2999–3011. https://doi.org/10.1016/j.jma.2023.09.003
38. Xhanari K, Finšgar M (2019) Organic corrosion inhibitors for aluminum and its alloys in chloride and alkaline solutions: A review. *Arab J Chem* 12: 4646–4663. https://doi.org/10.1016/j.arabjc.2016.08.009
39. Gobara M, Baraka A, Akid R, et al. (2020) Corrosion protection mechanism of Ce^{4+}/organic inhibitor for AA2024 in 3.5% NaCl. *RSC Adv* 10: 2227–2240. https://doi.org/10.1039/C9RA09552G

40. Zamani P, Valefi Z, Jafarzadeh K (2022) Comprehensive study on corrosion protection properties of Al_2O_3, Cr_2O_3 and Al_2O_3–Cr_2O_3 ceramic coatings deposited by plasma spraying on carbon steel. *Ceram Int* 48: 1574–1588. https://doi.org/10.1016/j.ceramint.2021.09.237

AIMS Press